Indian Journal of Chemistry
Vol. 56A, September 2017, pp. 913-924

Rhenium(I) complex with 2-(benzothiazol-2-yl) quinoline: Synthesis, characterization, spectral properties and DFT/TDDFT investigations

Rupa Sarkar, Debopam Sinha, Amit Maity & Kajal Krishna Rajak*

Department of Chemistry, Inorganic Chemistry Section, Jadavpur University, Kolkata 700 032, West Bengal, India

Email: kajalrajak@rediffmail.com; kkrajak@chemistry.jdvu.ac.in

Received 30 May 2016; revised and accepted 11 August 2017

The red colored mononuclear rhenium(I) complex having *fac*-$[Re(CO)_3]^+$ moiety of general formula, $[Re(CO)_3(N\cap N)Cl]$, has been synthesized in excellent yield by reacting $[Re(CO)_5Cl]$ with 2-(benzothiazol-2-yl) quinoline (1:1) in a boiling mixture of methanol+chloroform (3:1, *v/v*) under argon atmosphere. Elemental, ^1H and ^{13}C NMR analysis show the formation of the desired complex. The complex is also characterized by different spectroscopic techniques. The ground and excited-state geometries, NMR, absorption, and phosphorescence properties of the Re(I) complex are examined by DFT and TDDFT methods. The natural transition orbital and spin density difference map analysis reveals the nature of excitations. The lowest lying triplet excited state is associated with the ^{3}MLCT/^{3}ILCT excited state. The emission-like transition is consistent with the strong ^{3}MLCT/ ^{3}ILCT character.

Keywords: Coordination chemistry, Density functional calculations, Phosphorescence, Photophysical properties, ^{3}MLCT excited state, Natural transition orbitals, Electrochemical studies, Quinoline nitrogen, Rhenium

Controlling the behavior of singlet and triplet metal-to-ligand charge transfer (^{1}MLCT and ^{3}MLCT, respectively) excited states of transition metal complexes is key to their efficient use in photonic applications in the area of energy conversion,[1, 2] sensing[3–5] and molecular electronics.[6–8] In this connection, the metal complexes of heavy metal ions with d^6 configuration such as rhenium(I)[9] ruthenium(II)[10] osmium(II)[11] rhodium(III)[12] and iridium(III)[13] were studied[14] extensively by various techniques. For example, operation of Ir^{III} luminophores in organic light-emitting diodes (OLED),[15a, 15b] Ru^{II}-based sensitizers of solar cells[16,17] and Re^{I} probes of protein relaxation dynamics[18] and various luminescence sensors[18b] are all based on the presence of ^{3}MLCT states. Optical excitation of metal containing chromophores yields ^{1}MLCT states, from which the strongly phosphorescent triplet states are populated by intersystem crossing (ISC). It is to be noted that these metal ions show strong spin-orbit coupling as a result the triplet metal-to-ligand charge transfer excited state (^{3}MLCT) can emit molecular phosphorescence by borrowing the intensity of the singlet MLCT excited state.

Among these heavy metal ions, rhenium(I) complexes with the non innocent ligand bearing *fac*-$[Re(CO)_3]^+$ are of high interest.[19-21] Their unique combination of chemical stability, strong visible absorption, excited state reactivity, and photoredox chemistry and catalytic properties has stimulated efforts to exploit these compounds for solar energy conversion, light emitting devices, reduction of carbon dioxide in a homogeneous solution as well as at the electrode surfaces, chemi- or electro-chemiluminescence detectors and biological and medical diagnostics.[22-32]

In this context, the use of chelating ligands bearing quinoline nitrogen as a coordinating atom represents an important target when the coordination of transition metals is taken into consideration. The marked coordinating capability of the nitrogen coupled with the chromophoric characteristics of the quinoline ring induces the formation of stable metal complexes with potential photophysical properties.[33]

With the aforementioned in mind, we molecularly designed and synthesized the Re(I) quinolato complex (**1**) with *N, N* coordinating ligand having the imine function. The complex is characterized by IR, UV-vis, NMR (^{1}H and ^{13}C) spectroscopic techniques. The electrochemical behavior is also examined. The photophysical properties of the complex (**1**) were also investigated.

With the development of density functional theory (DFT) and especially the improvement of time-

dependent density functional theory (TDDFT)[34], properties of both ground- and excited-states for medium-sized metal complexes can be calculated at the first-principle level with good accuracy.[35, 36] To get better insight into the geometry and the electronic structure geometry, optimizations of the ground and excited-states were carried out by means of DFT calculations. We have also calculated and analyzed the singlet and triplet excited state natural transition orbitals (NTOs) derived from TDDFT results and compared with the ground state molecular orbitals (MOs) obtained by DFT calculations. The computational modeling of the NMR parameter is also of abiding interest, and such calculations at DFT has emerged as a promising approach for the prediction of nuclear shielding and coupling constants of NMR active nuclei.[37, 38] Thus, we have computed the proton and carbon NMR chemical shifts and also the ^{1}H-^{1}H spin-spin coupling constant using the gauge-independent atomic orbital (GIAO)-DFT method, which is aimed at providing the definitive characterization of the complex.

Materials and Methods

$[Re(CO)_5Cl]$ (98%), 2-quinolinecarboxaldehyde and 2-aminothiophenol used was purchased from Aldrich Chemical Co. All the chemicals and solvents were analytically pure and used without further purification.

UV-vis spectra were recorded on a Perkin-Elmer LAMBDA 25 spectrophotometer. IR spectra were obtained with a Perkin-Elmer L-0100 spectrophotometer. ^{1}H and ^{13}C NMR spectra were measured on a Bruker FT 300 MHz spectrometer and a Bruker FT 125 MHz spectrometer, respectively. Elemental analyses (C, H, N) were performed on Perkin-Elmer 2400 series II analyzer and electrochemical measurements were recorded on a CHI 620A electrochemical analyzer using platinum electrode under nitrogen atmosphere. Tetraethylammonium perchlorate (TEAP) was used as a supporting electrolyte and potentials were referenced to the Standard Calomel Electrode (SCE) without junction correction. The emission data were collected on a Horiba FluroMax-4 fluorescence spectrometer. For luminescence measurement excitation and emission slit width of 3 nm were used. Quantum yields of the complex was determined in freeze-pump-thaw-degassed solution of the complex by a relative method using $[Ru(bipy)_3]^{2+}$ in the same solvent as the standard[39]. The quantum yields[40] were calculated using Eq. (10),

$$\Phi_r = \Phi_{std} \frac{A_{std}}{A_r} \frac{I_r}{I_{std}} \frac{\eta_r^2}{\eta_{std}^2} \quad \ldots (1)$$

where Φ_r and Φ_{std} are the quantum yields of unknown and standard samples (Φ_{std} = 0.08951 at 298 K in CH_3CN at λ_{ex}= 450 nm), A_r and A_{std} (<0.1) are the solution absorbances at the excitation wavelength (λ_{ex}), I_r and I_{std} are the integrated emission intensities, and η_r and η_{std} are the refractive indices of the solvent. Experimental errors in the reported luminescence quantum yields were about 10%. Time-correlated single-photon-counting (TCSPC) measurements were carried out for the luminescence decay of complex in dimethyl suphoxide. For TCSPC measurement, the photoexcitation was made at 450 nm using a picosecond diode laser (IBH Nanoled-07) in an IBH Fluorocube apparatus. The fluorescence decay data were collected on a Hamamatsu MCP photomultiplier (R3809) and were analyzed by using IBH DAS6 software.

Computational details

The geometrical structures of the singlet ground state (S_0) and the lowest lying triplet excited state (T_1) were optimized by the DFT[41] method with B3LYP exchange correlation functional[42] approach. The geometry of the complex was fully optimized in solution phase without any symmetry constraints. The vibrational frequency calculations were also performed for the complex to ensure that the optimized geometry represents the local minima and there were only positive eigen values. There was good agreement between the theoretical and experimental structures. On the basis of the optimized ground and excited state geometry structures, the absorption and emission spectra properties in dimethyl sulfoxide (DMSO) media were calculated by time-dependent density functional theory (TDDFT)[43, 44] approach associated with the conductor-like polarizable continuum model (CPCM)[44]. We computed the lowest 50 singlet-singlet transition in ground state. Due to the presence of electronic correlations, the TDDFT (B3LYP) method can yield more accurate electronic excitation energies and hence, can provide a reasonable spectral feature for our complex of investigation.

In the calculations, the quasirelativistic pseudopotentials of Re atom proposed by Hay and Wadt[46] with 14 valence electrons (outer-core

[($5s^2 5p^6$)] electrons and the ($5d^6$) valence electrons) were employed, and a double-ξ quality basis set LANL2DZ was adopted as the basis set for Re atoms. For C, H, N, O, Cl and S atoms, we used 6-31+G(d, p) basis set for the optimization of both the ground state and the lowest lying triplet excited state geometries.

In addition, the ^{1}H and ^{13}C NMR properties of the complex (**1**) were calculated with the magnetic field perturbation method with the GIAO algorithm[47] with the NMR = spin-spin keyword incorporated in the Gaussian 09W program. In these calculations, the 6-311+G(2d,p) basis set was employed for all atoms other than rhenium. The relative chemical shift of a given nucleus X in the molecule was defined as δ_X^{calc} (ppm) = $\sigma_X^{calc} - \sigma_X^{ref}$, where TMS was used as a reference molecule optimized at the same level of theory.[47b,48a] To account for the solvent effect, we used the integral equation-formalism polarizable continuum model (IEFPCM) method.[48(b, c)]

Finally, to understand the nature of excited states involved in absorption and emission processes natural transition orbital (NTO) analysis was performed. This approach provides the most compact representation of the electronic transitions on terms of an expansion into single particle orbitals by diagonalizing the transition density matrix associated with each excitation.[49] The spin density difference map calculations were also performed to explain their optical properties. The figures showing MOs, NTOs and the difference density plots were prepared by using the GaussView 5.1 software. All the calculations were performed with the Gaussian 09W software package.[50] GaussSum 2.1 program[51] was used to calculate the molecular orbital contributions from groups or atoms. Natural bond orbital (NBO) calculations were performed with the NBO code[52] included in Gaussian 09.

Synthesis of complex

[$Re(CO)_3$(N∩N)Cl] (**1**) was synthesized as follows: To a stirred solution of 2-(benzothiazol-2-yl) quinoline (N∩N) (73 mg, 0.28 mmol) in 16 mL mixture of methanol and chloroform (3:1, *v/v*) [$Re(CO)_5Cl$] (101 mg, 0.28 mmol) was added and heated to reflux for 4-5 h under argon atmosphere. The solution turned orange and red colored crude product was obtained in good amount. After being cooled to room temperature the product was collected by suction filtration and washed with methanol and ether and allowed to dry in vacuum. The solid red mass was recrystallized from hot dimethylformamide. Yield: 120 mg (75%). Anal. (%): Calcd. for $C_{19}H_{10}ClN_2O_3ReS$: C, 50.63; H, 2.43; N, 6.75. Found: C, 50.75; H, 2.50; N, 6.85. IR_{exptl} (KBr, cm^{-1}): ν(Facial 3CO) 2014, 1920 and 1902. IR_{theor} (cm^{-1}): ν(Facial 3CO) 2010, 1913, 1901. ^{1}H NMR_{exptl} {300 MHz, DMSO-d_6, δ (ppm), *J* (Hz)}: 8.4 (H7, d, *J* = 11.2), 8.3 (H4, d, *J* = 10), 9.03 (H18, d, J = 11.3), 7.7–9.0 (10H, ArH). ^{1}H NMR_{theor} {δ (ppm), *J* (Hz)}: 7.5 (H7, d, *J* = 9.7), 8.4 (H4, d, *J* = 9.4), 9.0 (H18, d, *J* = 8.7), 7.3–9.0 (10H, ArH). ^{13}C NMR_{exptl} {125 MHz, DMSO-d_6, δ (ppm)}: 190.1, 198.9, 187.8 (3 CO's), 120.7–227.5 (16C, ArC). ^{13}C NMR_{theor} (δ (ppm)}: 229.6, 212.5, 227.5 (3 CO's), 123.3–229.5 (16C, ArC), E_{pa} (Re^{II}/Re^{I} couple): 1.06 V (irr), E_{pc} (ligand reduction couple): 0.05 V (irr) and E_{pc} (Re^{I}/Re^{0} couple): –0.19 V (irr),

Results and Discussion

Synthesis

The ligand 2-(benzothiazol-2-yl) quinoline (**I**) (general abbreviation (N∩N) was prepared according to the literature procedure[53] and were used as a *N*, *N* donor ligand for the preparation of the Re(I) complex (Scheme 1).

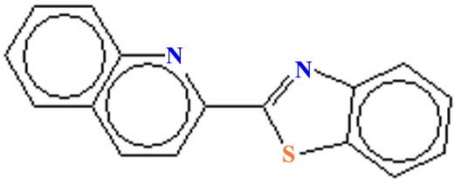

(I)

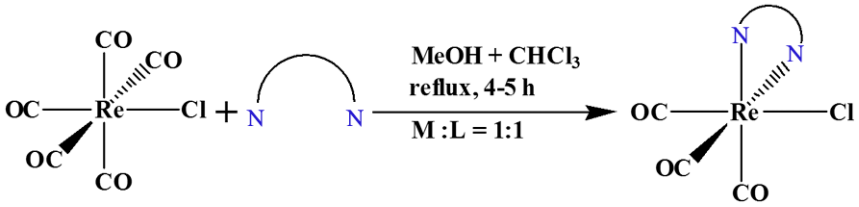

Schematic representation for the synthesis of the complex

Scheme 1

The stoichiometric reaction of $[Re(CO)_5Cl]$ with (N∩N) in a ratio of 1:1 boiling mixture of methanol and chloroform (3:1, *v/v*) under argon atmosphere afforded red colored mononuclear complex of general formula $[Re(CO)_3(N\cap N)Cl]$ (**1**) in good yield (Scheme 1). The elemental analysis and ^{1}H NMR and ^{13}C NMR spectroscopic measurements confirm the formation of the synthesized complex. (see Experimental section).

IR spectra

The IR spectra of the complex (**1**) were recorded on a KBr disk. The calculated IR spectra of the complex are reported. The complex shows three metal carbonyl stretching frequencies at 2014, 1920 and 1902 cm^{-1} which are consistent with the presence of *fac*-$[Re(CO)_3]^+$ core having pseudo-C_3v symmetry.

NMR spectra

The complex (**1**) is diamagnetic and display well-resolved ^{1}H and ^{13}C NMR spectra in DMSO solution. The assignment of NMR spectra is based on intensity and spin-spin splitting structure of Re(I) complex. In the complex, H4 and H7 are observed as doublet ~8.3 and 8.4 ppm, while H18 is observed as a doublet at 9.0 ppm. All the aromatic protons span in the range 7.7–9.0 ppm. The correlation between the experimental and calculated ^{1}H NMR chemical shift is shown in Fig. 1. The corresponding NMR spectrum of complex is given in Fig. S1 (Supplementary Data).

The complex shows three metal carbonyl resonances in the region 190.1, 198.9 and 187.8 ppm which corroborates the presence of pseudo C_3v *fac*-$[Re(CO)_3]^+$ core.[54] The differences in chemical shift values can be attributed to the π accepting property of nitrogen atoms. The complex shows two equatorial carbonyl groups near 198 ppm (*trans* to chlorine atom) and 190 ppm (*trans* to pyridyl moiety) while the axial carbonyl group is observed around 187 ppm (*trans* to N1 of ligand moiety). In the complex the aromatic carbons occur in the range 116–175 ppm. The calculated NMR spectral chemical shifts agree well with the experimental data. The experimental and calculated NMR data are given in the Experimental section.

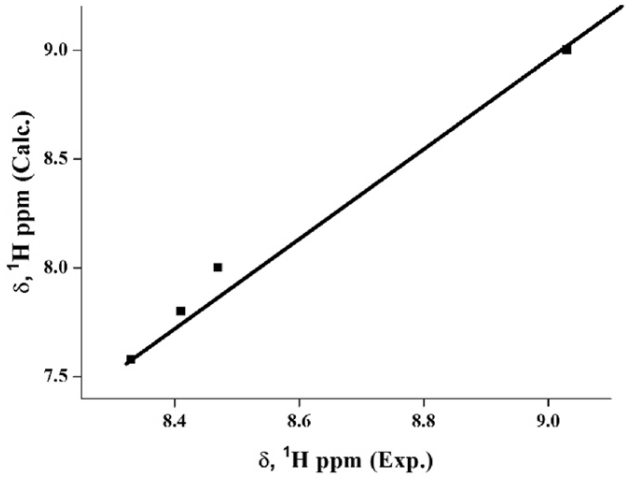

Fig. 1 – Linear correlation between the experimental and calculated ^{1}HNMR chemical shifts.

Geometry optimization, electronic structure

The complex (**1**) is diamagnetic at room temperature indicating its singlet ground state t_{2g}^6. The geometry optimization for the complex was performed in solution phases in their both ground singlet (S_0) and lowest lying excited triplet (T_1) spin state. The main optimized geometrical parameters are given in Table 1. The optimized structure of the complex at singlet ground state is shown in Fig. 2. The modeled geometries possess a distorted octahedral arrangement around the Re(I) center which are characterized by N1–Re1–C2 bond angle of 171.7°. The *fac*-$[Re(CO)_3]^+$ unit in complex (**1**) is nearly trigonal pyramid with ~90° angle between the CO ligands. From optimized geometry of the complex we know about the bond lengths of coordination sphere around metal center. In the complex the Re–C, Re–N1, Re–N2 and Re–Cl bond distances occur at around 1.92, 2.21, 2.28 and 2.55 Å, respectively.

Upon excitation, the complex (**1**) experiences vertical transition from ground state to singlet excited state and then undergo intersystem crossing to reach the triplet excited state in which emission might occur. According to structure-property relationship, the structural changes would be expected between the S_0 and T_1 states. The comparison of the S_0 and T_1 states geometries shows that, in the T_1 excited state, the metal-ligand bond lengths have perceptible changes.

The calculated Re–C bonds have about 0.04 Å elongations. The calculated bond angle C3–Re1–N2 shows only a slight change of about 3.4°. The calculated C=N bond distance in thiazole moiety occurs around 1.32 Å. In the T_1 state it occurs at ~1.37 Å. In the case of the ligand frame, the dihedral angle N2–C11–C10–S1 changes slightly by about 2.9°.

The partial frontier molecular orbital compositions and energy levels for complex in singlet ground state (S_0) are listed in Table 2. The partial molecular orbital

diagram and the partial molecular orbital diagram with some isodensity frontier molecular orbital which are mainly involved in the electronic transitions for complex are shown in Fig. 3. In the ground state (S_0), the HOMO (H) and H – 1 are at 0.12 eV. In our complex, the electron density in HOMO mainly resides on the metal (47%) along with carbonyl moiety (23%). There is also a small contribution from chlorine (19%) to HOMO. The H–1 is similarly composed [45% d(Re) + 21% π(CO) + 21% π(Cl)]. The energy difference between HOMO and LUMO (L) occurs at 3.279 eV. The H–2 of the complex lies at 0.504 eV below the HOMO. H–2 is mainly composed of 46% of quinoline moiety and 46% of

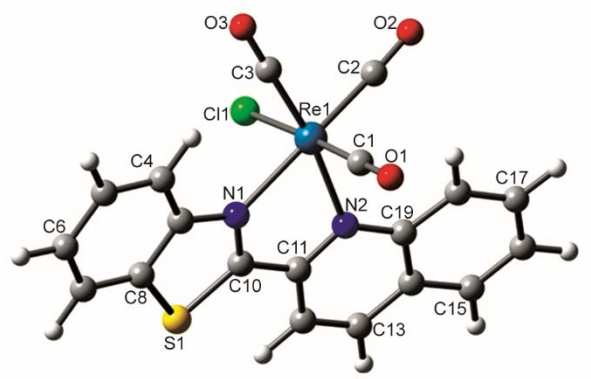

Fig. 2 – Optimized molecular structure of the complex (**1**) at S_0 state. [Re: Cyan, N: Blue, O: Red, Cl: Green, S: Yellow, C: Grey, H: White].

Table 1 – Selected optimized geometrical parameters for complex (**1**) in the ground (S_0) and lowest lying triplet (T_1) excited states at B3LYP levels

Bond lengths (Å)

	S_0	T_1		S_0	T_1
Re1–C1	1.913	1.950	Re1–N1	2.215	2.150
Re1–C2	1.926	1.958	Re1–N2	2.287	2.185
Re1–C3	1.917	1.952	C10–N1	1.318	1.374
Re1–Cl1	2.554	2.511	C10–S1	1.742	1.759

Bond angles (°)

	S_0	T_1		S_0	T_1
C2–Re1–N1	171.70	172.74	C1–Re1–Cl1	177.36	177.70
C3–Re1–N2	170.90	174.26	C2–Re1–Cl1	89.23	87.33
Cl1–Re1–C3	177.36	177.70	Cl1–Re1–N2	83.29	86.72
C3–Re1–N1	98.39	98.98	C1–Re1–N2	94.30	91.57
C1–Re1–N1	94.60	92.01	C2–Re1–N2	100.83	99.74
Cl1–Re1–N1	83.72	86.09			
N1–Re1–N2	74.05	76.82			
Cl1–Re1–C3	90.93	89.08			

Dihedral angle (°)

	S_0	T_1
N2–C11–C10–S1	173.42	176.36

Table 2 – Frontier molecular orbital composition (%) in the ground state for complex (**1**)

Orbital	Energy (eV)	Contribution (%)					Main bond type
		Re	CO	Ligand		Cl	
				Quinoline	Thiazole		
L+5	–0.811	0	1	51	47	0	π^*(L)
L+4	–0.967	1	6	9	83	0	π^*(L)
L+3	–1.209	26	56	6	12	0	p(Re)+π^*(CO)+ π^*(L)
L+2	–1.275	35	50	6	9	0	p(Re)+π^*(CO)
L+1	–1.951	0	1	79	20	0	π^*(L)
L	–3.201	2	3	56	39	1	π^*(L)
H	–6.480	47	23	4	7	19	d(Re)+π(CO)+π(Cl)
H-1	–6.605	45	21	8	5	21	d(Re)+π(CO)+π(Cl)
H-2	–6.984	7	3	46	37	7	π(L)
H-3	–7.049	60	27	3	10	1	d(Re)+π(CO)+π(L)
H-4	–7.154	3	1	36	58	2	π(L)
H-5	–7.210	1	1	39	43	16	π(L)+π(Cl)

quinoline moiety of π(L). The H−3 and H−4 are almost degenerate (energy difference ~0.1 eV). LUMO (L) and L+1 of the complex originates from ligand π^* orbital, mainly localized on quinolone part of ligand moeity. L+2 orbital shows a strong contribution of the π^*(CO) along with metal *p* orbital.

The lowest lying excited triplet (T_1) state optimized structure of the complex (**1**) is given in Fig. S2 (Supplementary Data) and the significant geometrical parameters in the T_1 state for complex (**1**) are listed in Table 1 while the isodensity surfaces of the highest and lowest singly occupied molecular orbitals (HSOMO and LSOMO respectively) at the relaxed T_1 geometry is shown in Fig. 4. Also, the corresponding electrons spin density, which is defined as the difference between α and β spin contributions to the total electron density, are depicted in Fig. 4.

The analysis of the singly occupied molecular orbitals at the T_1 geometry showed that the LSOMO is mainly located on the metal and resembles the HOMO of the corresponding S_0 geometry. On the other hand, π orbital of ligand contributes primarily to HSOMO along with a very small contribution arises from the metal and HSOMO strongly resembles the corresponding LUMO and L+1 of the S_0 geometry.

It is clear from spin density plot that the spin density is mainly localized on the both ligand and Re(I). Thus, the lowest-lying triplet excited state (T_1) is the admixture of (^{3}MLCT) and (^{3}ILCT) excited state.

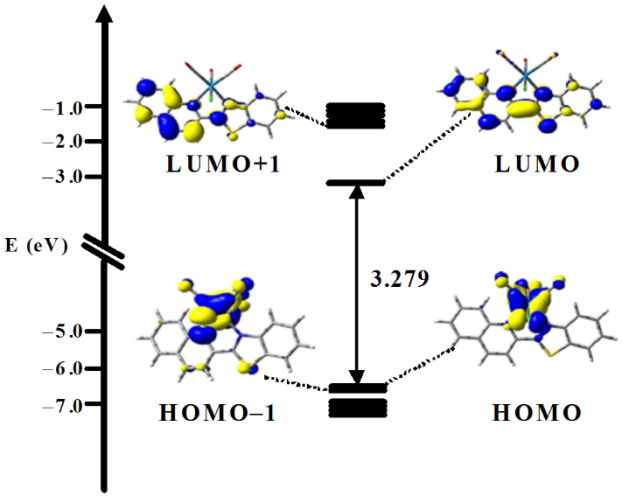

Fig. 3 – Left: Partial molecular orbital diagram for the complex (**1**). The arrows indicate the HOMO−LUMO energy gaps. Right: Partial molecular orbital diagram with some isodensity frontier molecular orbital mainly involved in the electronic transitions for complex (**1**).

Charge distribution and NBO analysis

Table 3 represents the atomic charges from the Natural Population Analysis (NPA) for complex (**1**). The calculated charge on the rhenium atom is considerably lower than the formal charge of +1. This difference is a result of significant charge donation from the Cl, $N_{pyridyl}$, $N_{S.b}$. The charge on the N-donor center is significantly smaller and less negative than the charge on the Cl atom, indicating that there is higher electron density delocalization from the N-donor center to rhenium.

The nature of bonding interactions in the complex has been studied by NBO analysis. The occupancy and the composition of the calculated Re–CO natural bond orbitals (NBOs) for complex are given in Table 4. The Re–$N_{S.b}$ bond orbital for complex was not detected, indicating a conceivable predominant Coulomb-type Re–ligand interaction.

Each natural bond orbital (NBO) σ_{AB} can be written in terms of two directed valence hybrids (NHOs) h_A and h_B on atoms *A* and *B*,

Table 3 – Atomic charges from the natural population analysis (NPA) for complex (**1**)

Atom	Atomic charge
Re	–0.8572
$N_{pyridyl}$	–0.3804
$N_{S.b}$	–0.3950
Cl	–0.4876

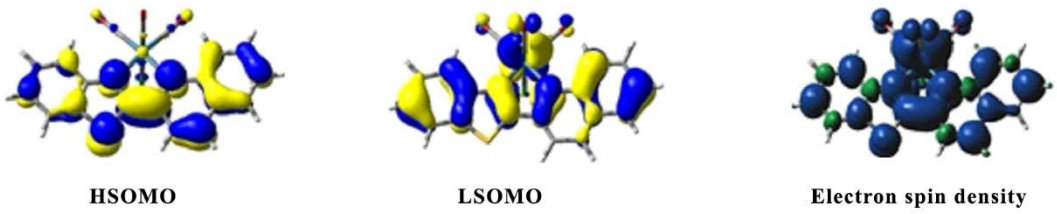

Fig. 4 – Isodensity surface plots of the highest and lowest singly occupied molecular orbitals, HSOMO and LSOMO, respectively, along with the corresponding electron spin density at T_1 state geometry. [Blue and green colors show regions of positive and negative difference between the alpha and beta electron densities, respectively].

Table 4 – The occupancies and composition of the calculated natural bond orbitals (NBOs) for complex (**1**)

BD	Occupancy	Composition of NBO	BD	Occupancy
Re–CO (1)	1.9229	$0.5934(spd)_{Re} + 0.8049(sp)_C$	$0.8049(spd)_{Re} - 0.5934(sp)_C$	0.1195
Re–CO (2)	1.9620	$0.6149(spd)_{Re} + 0.7886(sp)_C$	$0.7886(spd)_{Re} - 0.6149(sp)_C$	0.2141
Re–CO (3)	1.9628	$0.6191(spd)_{Re} + 0.7853(sp)_C$	$0.7853(spd)_{Re} - 0.6191(sp)_C$	0.2068

Table 5 – Photophysical parameters of complex (**1**) in dimethyl sulphoxide solution at room temperature

λ_{max} (nm) (ε, M^{-1} cm^{-1})	λ_{emi} (nm)	Φ ($\times10^{-3}$)	$k_r \times10^5$ (s^{-1})	$k_{nr}\times10^8$ (s^{-1})	τ_1 (ns)	τ_2 (ns)
424 (4543), 373 (26695), 299 (12978), 276 (15847)	438	2.79	4.21	1.51	1.27	6.62

Table 6 – Main calculated optical transition for the complex (**1**) with composition in terms of molecular orbital contribution of the transition, vertical excitation energies, and oscillator strength in dimethyl sulphoxide

Electronic Transitions	Composition	Excitation energy (eV)	Oscillator strength (*f*)	CI	Assignment	λ_{exp} (nm)
$S_0 \rightarrow S_2$	H –1 → L	2.7493 (450 nm)	0.0783	0.6968	^{1}MLCT / ^{1}ILCT	424
$S_0 \rightarrow S_4$	H –5 → L	3.3005 (375 nm)	0.2461	0.10525	^{1}MLCT / ^{1}ILCT	373
	H –4 → L			0.21801	^{1}MLCT / ^{1}ILCT	
	H –3 → L			0.24519	^{1}MLCT / ^{1}ILCT	
	H –2 → L			0.60677	^{1}MLCT / ^{1}ILCT	
$S_0 \rightarrow S_{11}$	H –3 → L +	4.1301 (300 nm)	0.0291	–0.1715	^{1}MLCT / ^{1}ILCT	299
	H → L + 2			0.62740	^{1}MLCT / ^{1}ILCT	
$S_0 \rightarrow S_{15}$	H –8→ L	4.4488 (278 nm)	0.0309	0.13573	^{1}ILCT	276
	H –3 → L +			0.52205	^{1}MLCT / ^{1}ILCT	
	H –2 → L +			–0.3459	^{1}ILCT	
	H –1 → L +			0.20016	^{1}MLCT / ^{1}ILCT	

$$\sigma_{AB} = c_A h_A + c_B h_B$$

where c_A and c_B are polarization coefficients. Each valence bonding NBO must in turn be paired with a corresponding valence *anti*-bonding NBO,

$$\sigma^*_{AB} = c_A h_A - c_B h_B$$

to complete the span of the valence space. The Lewis-type (donor) NBOs are thereby complemented by the non-Lewis-type (acceptor) NBOs that are formally empty in an idealized Lewis picture.

The interactions between 'filled' Lewis-type NBOs and 'empty' Lewis-type NBOs lead to loss of occupancy from the localized NBOs of the idealized Lewis structure into the empty non-Lewis orbitals, and they are referred to as 'delocalization' corrections to the zeroth-order natural Lewis structure.[55] The NBO analysis of complex confirms one bond orbital for all Re–CO. The *s*, *p* and *d* orbitals of rhenium participate in the formation of all Re–CO bonds.

Absorption spectral properties

The absorption spectra of the complex (**1**) were recorded in dimethyl sulphoxide (DMSO) solution at room temperature and showed absorption maxima at 424, 373, 299, 276 nm. Higher energy absorption features in the UV portion of the spectrum are assigned to ILCT (π–π^*) absorptions while the lower energy UV bands are assigned to MLCT transition. The absorption bands in the region 299–424 nm for the complex can reasonably be assigned to an admixture of metal-to-ligand charge-transfer (^{1}MLCT) transition and spin-allowed $\pi\rightarrow\pi^*$ (ligand centered, ^{1}ILCT) transitions. These assignments were supported by theoretical calculations (from spin density plot and also from natural transition orbital (NTO) analysis).

Figure 5 show the experimental absorption spectra for complex (**1**). The photophysical parameters of the complex are given Table 5. The calculated absorption energies associated with their oscillator strengths, the main configurations and their assignments as well as the experimental result is given in Table 6. Table 6 confirms the usual assignments of all the absorption bands. The accompanying electron density redistributions in complex are shown in Fig. 6. From the spin density plot, we can conclude that the absorption bands in the region 276–424 nm for complex have mixed ^{1}MLCT and ^{1}ILCT character.

In order to analyze the nature of absorption, we performed an NTO analysis based on the calculated transition density matrices.[49] This method offers the most compact representation of the transition density between the ground and excited states in terms of an expansion into single-particle transitions (hole and electron states for each given excitation). Here we refer to the unoccupied and occupied NTOs as ''electron'' and ''hole'' transition orbitals, respectively. Note that NTOs are not the same as virtual and occupied MO pairs from the ground state calculations. Figure 7 illustrates the natural transition orbitals (NTOs) for the complex. Based on our TDDFT NTOs analysis the bands in the region 276–424 nm can be characterized as a mixture of MLCT and ILCT states. As illustrated in Fig. 7, optical excitations occur from the occupied (hole) transition orbitals to the unoccupied (electron) transition orbitals. Hole NTOs contributing to the bands are localized on the Re center along with π orbitals of ligands (t_{2g}–π), while the electron NTOs are mainly delocalized over the π*orbital of the ligand moiety.

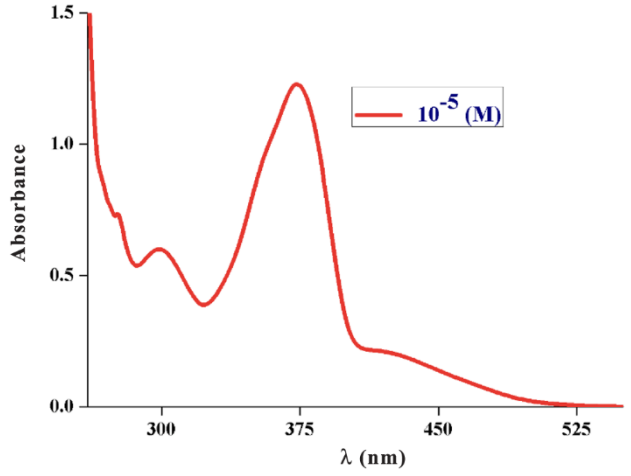

Fig. 5 – Experimental absorption spectra of the complex (**1**) in DMSO solution at room temperature.

Emission spectral properties

The emission spectral behavior of complex (**1**) was studied at room temperature in DMSO solution. The photophysical parameters are listed in Table 5. Figure 8 represents the emission spectra of the complex in DMSO solution. The complex upon excitation at the wavelength where the MLCT absorption maxima was observed, exhibits broad luminescent maxima at 438 nm in DMSO at room temperature. The bands have the characteristics of emission from the ^{3}MLCT excited state, which corresponds to a spin-forbidden Re→L transition.[56, 57] At room temperature in solution state, this complex is a weak emitter having quantum yield of 2.79×10^{-3}.

Time resolved luminescence spectra is an important tool to understand the decay process and the emissive nature of the complex. Thus, time resolved luminescence spectra were recorded for the complex. The complex (**1**) displays a bi-exponential decay nature and the decay plot is shown in Fig. 9. The fluorescence life time (τ), radiative (k_r) and nonradiative (k_{nr}) decay rate constant are collected in Table 5. The photoluminescence property mainly originates from triplet state charge transfer transitions. Thus, the lowest lying triplet state geometry of the complex was optimized using unrestricted B3LYP method in solution phase and selected geometrical parameters are depicted in Table 1. The calculated results reveal that the geometrical parameters are slightly from those of the ground state structures.

Figure 10 illustrates the natural transition orbitals (NTOs) for the Re complex. Based on our TDDFT NTOs analysis at T_1 state, the emission band for complex was characterized as ^{3}MLCT/^{3}ILCT transitions. Table 7 describes the calculated emission energies associated with their oscillator strengths, the main configurations and their assignments as well as the experimental result. TDDFT study at T_1 state for complex corroborates with the ^{3}MLCT/ ^{3}ILCT nature for all the transitions.

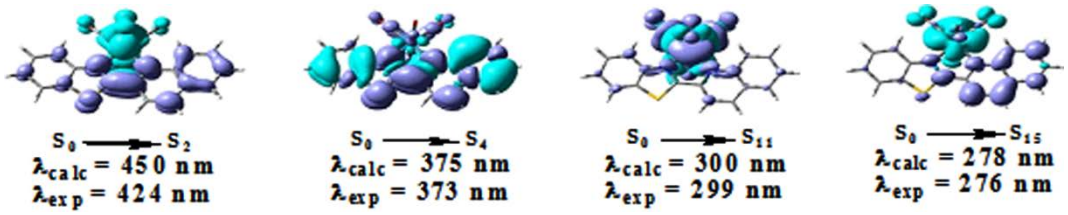

Fig. 6 – Difference electron density upon excitation from the ground state (S_0) to allowed singlet states (40 singlet to singlet excitations) for complex determined with TD-DFT (B3LYP/CPCM-DMSO) calculations. [Turquoise and purple colors show regions of decreasing and increasing electron density, respectively].

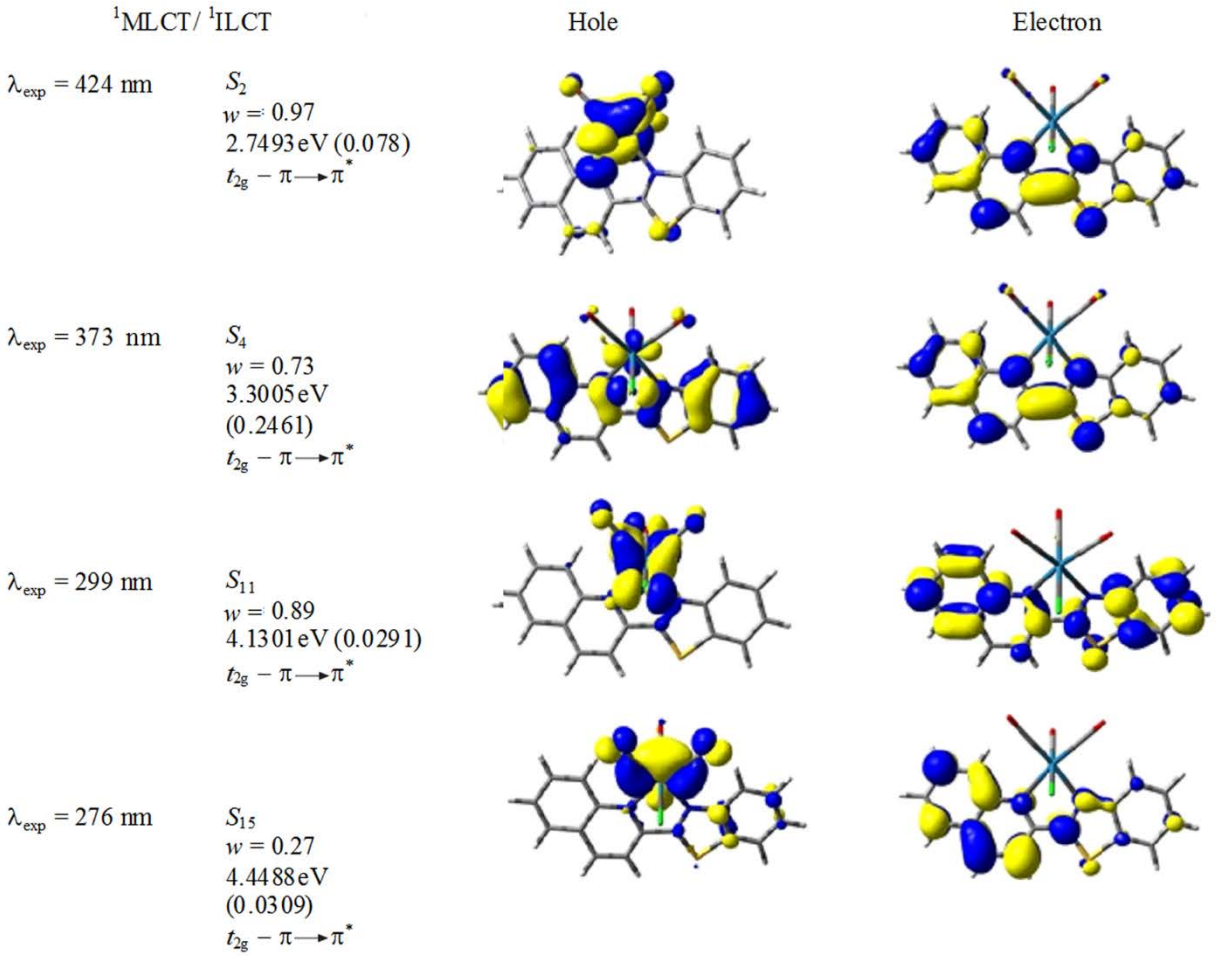

Fig. 7 – Natural transition orbitals (NTOs) for the complex (**1**) illustrating the nature of optically active singlet excited states in the absorption bands, 424, 373, 299 and 276 nm. For each state, the respective number of the state, transition energy (eV), and the oscillator strength (in parentheses) are listed. Only occupied (holes) and unoccupied (electrons) NTO pairs that contribute more than 25% to each excited state are shown. All transitions are mixed ^{1}MLCT/^{1}ILCT character: charge is transferred from $t_{2g} - \pi$ hole orbital to the π^* orbital of the ligands.

Table 7 – Calculated triplet excited state of complex (**1**) in dimethyl sulphoxide based on the lowest lying triplet state geometry. Main calculated vertical transitions with compositions in terms of molecular orbital contribution of the transition , vertical excitation energies and oscillator strength

Excitation	Comp.	Excitation energy (eV)	Oscillator strength (f)	CI	Assignment	λ_{exp} (nm)
1	H → L + 4	2.7509	0.0630	0.20966	^{3}MLCT/^{3}ILCT	438
	H → L + 5	(450 nm)		0.16949	^{3}MLCT/^{3}ILCT	
	H – 10 → L			–0.12599	^{3}MLCT/^{3}ILCT	
	H – 9 → L			0.28505	^{3}MLCT/^{3}ILCT	
	H – 8 → L			0.15977	^{3}MLCT/^{3}ILCT	
	H – 2 → L + 1			0.12059	^{3}MLCT/^{3}ILCT	
	H → L + 1			0.70070	^{3}MLCT/^{3}ILCT	

Electrochemical studies

Cyclic voltammetry was carried out for the complex (**1**) in dimethyl sulphoxide solution at room temperature under nitrogen atmosphere with tetraethylammonium perchlorate (TEAP) as the supporting electrolyte using a Pt electrode as working electrode. The potentials are referenced to the saturated calomel electrode (SCE) without junction correction. The complex exhibited two irreversible reduction waves at 0.05 and –0.19 V. The single ligand centered reduction wave observed at 0.05 V and the second wave observed for complex at –0.19 V

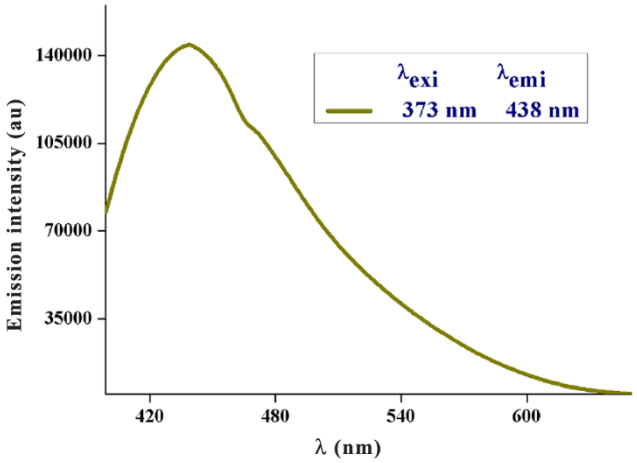

Fig. 8 – Emission spectra of complex (**1**) in dimethyl sulphoxide solution at room temperature.

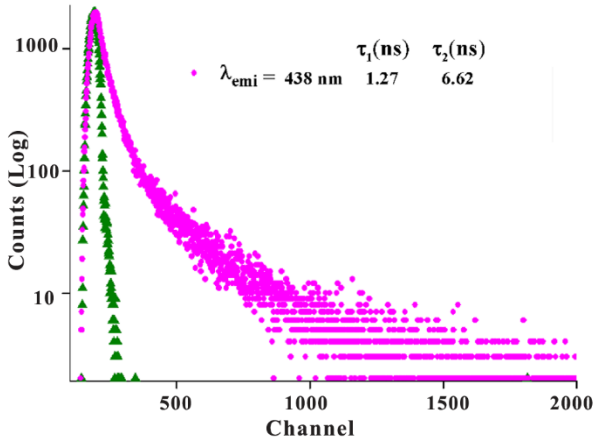

Fig. 9 – Changes in the time-resolved photoluminescence decay of complex (**1**) in DMSO at room temperature obtained with 373 nm excitation. [The emission at 438 nm was monitored].

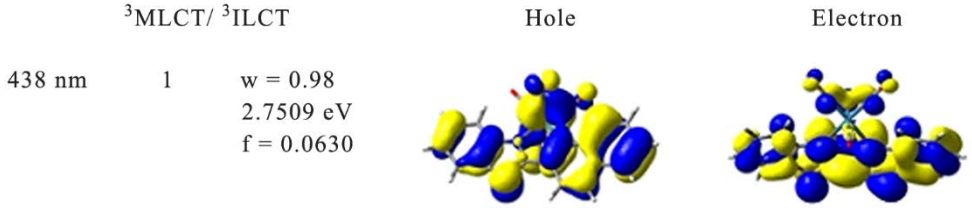

Fig. 10 – Natural transition orbitals (NTOs) for complex (**1**) illustrating the nature of optically active triplet excited state in the emission band of 438 nm. For each state, the transition energy (eV), and the oscillator strength (f) are listed. Only occupied (holes) and unoccupied (electrons) NTO pairs that contribute more than 25% to the excited state are shown. The transition has ^{3}MLCT /^{3}ILCT character.

are due to reduction of Re(I) to Re(0).[58a, b] An irreversible metal centered oxidation wave for Re^{II}/Re^{I} redox couple occurred at 1.06 V. A representative voltammogram is given in Fig. S3 (Supplementary Data). The electrochemical data is depicted in Experimental section. It has been reported earlier[59] that the study of electrochemical behavior is an important phenomenon of the complexes where HOMO and LUMO orbitals were involved in the redox processes. HOMO of the studied complex consists of nearly 47% rhenium *d*-orbital, 19% chloro and 23% carbonyl character, while the LUMO is mainly localized on the ligand. Thus, the oxidation (~1.06 V), i. e. the removal of electron from orbital containing a metal *d* character with a considerable contribution from Cl and carbonyl moiety is probably responsible for irreversible electrochemical behavior. On the other hand, the one electron reduction (near 0.05 V) involved addition of one electron to the π* orbital of the ligand moiety.

Conclusions

In summary, we have synthesized a rhenium tricarbonyl complex with 2-(benzothiazol-2-yl) quinoline (**1**). The present work investigated the ground- and excited-state geometries, NMR, absorption, and phosphorescence properties of this Re(I) complex by DFT and TDDFT methods. TDDFT investigations gave an insight into the optical transitions involved in the excitation process. From the calculated results, we have characterized all of the low-lying electronic states as admixture of ILCT and MLCT in character. The nature of the transitions was also supported by spin density difference map and natural transition orbital (NTO) analysis. The emission-like transition is associated with strong ^{3}MLCT character, as demonstrated by electron spin density.

Supplementary Data

Supplementary Data associated with this article are available in the electronic form at http://www.niscair.res.in/jinfo/ijca/IJCA_56A(09)913-924_SupplData.pdf.

Acknowledgement

Financial assistance received from the Council of Scientific and Industrial Research, New Delhi, India, Science & Engineering Research Board, New Delhi,

India is gratefully acknowledged. We are also thankful to Department of Science and Technology, New Delhi, India for the data collection on the CCD facility setup (Jadavpur University) under DST-FIST program. We also acknowledge CAS, Department of Chemistry, Jadavpur University and DST-PURSE program for other facilities. RS and AM are also thankful to UGC, New Delhi for the research fellowship.

References

1 Grätzel M, *Acc Chem Res,* 42 (2009) 1788.
2 Song W J, Chen Z F, Brennaman M K, Concepcion J J, Patrocinio A O T, Murakami Iha N Y & Meyer T J, *Pure Appl Chem*, 83 (2011) 749.
3 Kumar A, Sun S S & Lees A J, *Photophysics and photochemistry of organometallic rhenium diimine complexes*, in *Topics in Organometallic Chemistry*, Vol. 29, edited by A J Lees, (Springer, New York) 2010, p. 1.
4 Itokazu M K, Polo A S & Murakami Iha N Y, *J Photochem Photobiol A*, 160 (2003) 27.
5 Wagenknecht P S & Ford P C, *Coord Chem Rev*, 255 (2011), 591.
6 Hugel T, Holland N B, Cattani A, Moroder L, Seitz M & Gaub H E, *Science*, 296 (2002) 1103.
7 Balzani V, Credi A & Venturi M, *ChemPhysChem*, 9 (2008) 202.
8 Santoni M P, Hanan G S, Hasenknopf B, Proust A, Nastasi F, Serroni S & Campagna S, *Chem Commun*, 47 (2011) 3586.
9 (a) Dominey R N, Hauser B, Hubbard J & Dunham J, *Inorg Chem*, 30 (1991) 4754; (b) Sacksteder L, Lee M, Demas J N & DeGraff B A, *J Am Chem Soc*, 115 (1993) 8230; (c) Sarkar R, Mondal P & Rajak K K, *Dalton trans,* 43 (2014) 2859; (d) Sarkar R &. Rajak K K, *J Organomet Chem*, 779 (2015) 1.
10 (a) Smothers W K & Wrighton M S, *J Am Chem Soc*, 105 (1983) 1067; (b) Wang Y S, Liu S X, Pinto M R, Dattelbaum D M, Schoonover J R & Schanze K S, *J Phys Chem A*, 105 (2001) 11118.
11 Tung Y L, Wu P C, Liu C S, Chi Y, Yu J K, Hu Y H, Chou P T, Peng S M, Lee G H, Tao Y, Carty A J, Shu C F & Wu F I, *Organometallic*s, 23 (2004) 3745.
12 Shinozaki K & Takahashi N, *Inorg Chem*, 35 (1996) 3917.
13 Lamansky S, Djurovich P, Murphy D, Abdel-Razzaq F, Lee H E, Adachi C, Burrows P E, Forrest S R & Thompson M E, *J Am Chem Soc*, 123 (2001) 4304.
14 *Luminescent Organometallic Compound and Light Emitting Device*, US Patent, 2006, Patent no. 7067202 B2.
15 (a) Evans R C, Douglas P & Winscom C, *J Coord Chem Rev*, 250 (2006) 2093; (b) Yersin H, *Triplet Emitters for OLED Applications. Mechanisms of Exciton Trapping and Control of Emission Properties*, In *Topics in Current Chemistry: Transition Metal and Rare Earth Compounds*, Vol. 241, (Springer, New York) 2004, pp. 1-26.
16 Hagfeldt A & Grätzel M, *Acc Chem Res*, 33 (2000) 269.
17 Grätzel M, *Nature*, 414 (2001) 338.
18 Blanco-Rodríguez A M, Busby M, Grădinaru C, Crane B R, Di Bilio A J, Matousek P, Towrie M, Leigh B S, Richards J H, Vlček A Jr & Gray H B, *J Am Chem Soc*, 128 (2006) 4365.
19 Wrighton M S & Morse D L, *J Am Chem Soc*, 96 (1974) 998.
20 Kirgan R A, Sullivan B P & Rillema D P, *Topics Curr Chem*, 281 (2007) 45.
21 Richter M M, *Chem Rev*, 104 (2004) 3003.
22 Zipp A P, *Coord Chem Rev*, 84 (1988) 47.
23 Balzani V & Scandola F, *Supramolecular Photochemistry*, (Ellis Horwood, Chichester) 1991.
24 Caspar J V, Sullivan B P & Meyer T J, *Organometallics*, 5 (1986) 1500.
25 Carbera C R & Abruna H D J, *Electroanal Chem Interfacial Electrochem*, 209 (1986) 101.
26 (a) Oriskovich T A, White P S & Thorp H H, *Inorg Chem*, 34 (1995) 1629; (b) Connick W B, Bilio A J D, Hill M G, Winkler J R; Gray H B, *Inorg Chim Acta*, 240 (1995) 169.
27 Bhattacharyya S & Dixit M, *Dalton Trans*, 40 (2011) 6112.
28 Sundararajan C, Besanger T R, Labiris R, Guenther K J, Strack T, Garafalo R, Kawabata T T, Finco-Kent D, Zubieta J, Babich J W & Valliant J F, *J Med Chem*, 53 (2010) 2612.
29 de Silva A P, Fox D B, Huxley A J M, McClenagan N D & Roiron J, *Coord Chem Rev*, 185-186 (1999) 297.
30 Desvergne J P, Czarnik A W, *Chemosensors of Ions and Molecules*, *NATO ASI-C Series*, (Kluwer, Dordrecht, Germany) 1997.
31 Demas J N & DeGraff B A, *Anal Chem* 63 (1991) 829A.
32 Demas J N & DeGraff B A, *Coord Chem Rev*, 211 (2001) 317.
33 (a) Fahrni C J & Halloran T V O, *J Am Chem Soc*, 121 (1999) 11448; (b) Thompson R B, *Curr Opin Chem Biol*, 9 (2005) 526; (c) Chien T C, Dias L G, Arantes G M, Santos L G C, Triboni E R, Bastos E L & Politi M J, *J Photochem Photobiol A*, 194 (2008) 37; (d) Quang D T & Kim J S, *Chem Re*, 110 (2010) 6280; (e) Zhang J F & Kim J S, *Anal Sci*, 25 (2009) 1271.
34 Marques M A L & Gross E K U, *Annu Rev Phys Chem*, 55 (2004) 427.
35 Wang Y, Wang Y, Wang J, Liu Y & Yang Y, *J Am Chem Soc*, 131 (2009) 8839.
36 Gao X, Wang Y, Wang Y, Jia J & Su X, *Sci Sin Chim*, 41 (2011) 1145.
37 (a) Wolinski K, Hinton J F & Pulay P, *J Am Chem Soc* 112 (1990) 8251; (b) Taehtinen P, Bagno A, Klika K & Pihlaja K, *J Am Chem Soc*, 125 (2003) 4609; (c) Cloran F, Carmichael I & Serianni A S, *J Am Chem Soc*, 123 (2001) 4781.
38 (a) Mondal P, Hens A, Basak S & Rajak K K, *Dalton Trans*, 42 (2013) 1536; (b) Basak S, Chopra D & Rajak K K, *J Organomet Chem*, 693 (2008) 2649.
39 (a) Sullivan B P, Salmon D J, Meyer T J & Peedrin J, *Inorg Chem*, 18 (1979) 3369; (b) Juris A, Balzani V, Barigelletti F, Campagna S, Besler P, von Zelewsky A, *Coord Chem Rev*, 84 (1988) 85.
40 van Houten J & Watts R J, *J Am Chem Soc*, 98 (1976) 4853.
41 Runge E & Gross E K U, *Phys Rev Lett*, 52 (1984) 997.
42 (a) Becke A D, *J Chem Phys*, 98 (1993) 5648; (b) Lee C, Yang W & Parr R G, *Phys Rev B*, 37 (1988) 785.
43 (a) Casida M E, Jamoroski C, Casida K C & Salahub D R, *J Chem Phys*, 108 (1998) 4439; (b) Stratmann R E, Scuseria G E & Frisch M J, *J Chem Phys*, 109 (1998) 8218; (c) Bauernschmitt R & Ahlrichs R, *Chem Phy Lett*, 256 (1996) 454.

44 (a) Barone V & Cossi M, *J Phys Chem A*, 102 (1998) 1995; (b) Cossi M & Barone V, *J Chem Phys*, 115 (2001) 4708; (c) Cossi M, Rega N, Scalmani G & Barone V, *J Comp Chem*, 24 (2003) 669.

45 (a) Liu T, Zhang H X & Xia B H, *J Phys Chem A*, 111 (2007) 8724; (b) Zhou X, H.X. Zhang, Pan Q J, Xia B H & Tang A C, *J Phys Chem A*, 109 (2005) 8809; (c) Zhou X, Ren A M & Feng J K, *J Organomet Chem*, 690 (2005) 338; (d) Albertino A, Garino C, Ghiani S, Gobetto R, Nervi C, Salassa L, Rosenverg E, Sharmin A, Viscardi G, Buscaino R, Cross G & Milanesio M, *J Organomet Chem*, 692 (2007) 1377.

46 (a) Hay P J & Wadt W R, *J Chem Phys*, 82 (1985) 270; (b) Hay P J & Wadt W R, *J Chem Phys*, 82 (1985) 299.

47 (a) Wolniski K, Hilton J F & Pulay P, *J Am Chem Soc*, 112 (1990) 8251; (b) Ditchfield R, *Mol Phys*, 27 (1974) 789; (c) Mcweeny R, *Phys Rev* 126 (1962) 1028; (d) London F, *J Phys Chem*, (1937) 397.

48 (a) Rohlfing C M, Allen L C & Ditchfield R, *Chem Phys*, 87 (1984) 9; (b) Cossi M, Barone V, Mennucci B & Tomasi J, *Chem Phys Lett*, 286 (1998) 253; (c) Cancès E, Mennucci B & Tomasi J, *J Chem Phys*, 107 (1997) 3032.

49 Martin R L, *J Chem Phys*, 118 (2003) 4775.

50 *Gaussian 09*, *rev. A.1*, (Gaussian, Inc., Wallingford, CT) 2009.

51 O'Boyle N M, Tenderholt A L & Langner K M, *J Comp Chem*, 29 (2008) 839.

52 Glendening E D, Reed A E, Carpenter J E & Weinhold F, *NBO*, *ver. 3.1*, (University of Wisconsin, Madison, USA) 1995.

53 Gangopadhyay J, Sengupta S, Bhattacharyya S, Chakraborty I & Chakravorty A, *Inorg Chem*, 41 (2002) 2616.

54 (a) Mondal P, Hens A, Basak S, Rajak K K, *Dalton Trans*, 42 (2013) 1536; (b) Basak S, Chopra D & Rajak K K, *J Organomet Chem*, 693 (2008) 2649.

55 Reed E, Curtiss L A & Weinhold F, *Chem Rev*, 88 (1988) 899.

56 Juris A, Balzani V, Barigelletti F, Campagna S, Belser P, von Zelewsky A, *Coord Chem Rev*, 84 (1988) 85.

57 Kalyansundaram K, *Photochemistry of Polypyridine and Porphyrin Complexes*; (Academic Press, London) 1992.

58 (a) Juris A, Campagna S, Bidd I, Lehn J M & Ziessel R, *Inorg Chem*, 27 (1988) 4007; (b) Luong J C, Nadjo L & Wrighton M S, *J Am Chem Soc*, 100 (1978) 5790.

59 Wallace L & Rillema D P, *Inorg Chem*, 32 (1993) 3836.